Mechanistic Insights into the Propagation Cycle of the Hofmann–Löffler–Freytag Reaction. Halogen *vs* Hydrogen Atom Transfer

Journal:	*The Journal of Organic Chemistry*
Manuscript ID	jo-2024-02997q.R3
Manuscript Type:	Article
Date Submitted by the Author:	n/a

Complete List of Authors:	Zubcic, Gabrijel; University of Zagreb Faculty of Pharmacy and Biochemistry Andrijanić, Luka; University of Zagreb Faculty of Science Dzeba, Iva; Institut Ruder Boskovic You, Jiangyang; Institut Ruder Boskovic, Division of Physical Chemistry Friganović, Tomislav; Sveuciliste u Zagrebu, Faculty of Pharmacy and Biochemistry Portada, Tomislav; Institut Ruder Boskovic Pavic, Kristina; University of Zagreb Faculty of Pharmacy and Biochemistry Bešic, Erim; University of Zagreb, Vrcek, Valerije; University of Zagreb Faculty of Pharmacy and Biochemistry, Department of Organic Chemistry Šakić, Davor; University of Zagreb Faculty of Pharmacy and Biochemistry, Department of Analytical Chemistry

Mechanistic Insights into the Propagation Cycle of the Hofmann–Löffler–Freytag Reaction. Halogen *vs* Hydrogen Atom Transfer

Gabrijel Zubčić,[1] Luka Andrijanić,[2] Iva Džeba,[3] Jiangyang You,[3] Tomislav Friganović,[2] Tomislav Portada,[3] Kristina Pavić,[1] Erim Bešić,[1] Valerije Vrček,[1] and Davor Šakić[1,]*

[1] University of Zagreb Faculty of Pharmacy and Biochemistry, Ante Kovačića 1, 10000 Zagreb, Croatia

[2] University of Zagreb Faculty of Science, Horvatovac 102 a, 10000 Zagreb, Croatia

[3] Ruđer Bošković Institute, Bijenička cesta 54, 10000 Zagreb, Croatia

AUTHOR INFORMATION

Corresponding Author

*Davor Šakić − University of Zagreb Faculty of Pharmacy and Biochemistry, Ante Kovačića 1, 10000 Zagreb, Croatia; orcid.org/0000-0002-8871-6622; e-mail: davor.sakic@pharma.unizg.hr

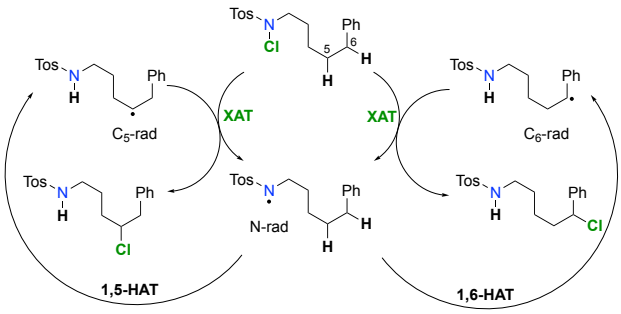

ABSTRACT:

The Hofmann–Löffler–Freytag (HLF) reaction is a method that employs N-chlorinated precursors in radical-mediated rearrangement cycles to synthesize pyrrolidine rings and C–H functionalised products. This study aims to elucidate the mechanism of the propagation cycle, identify the rate-limiting step, and uncover the factors influencing the regioselectivity of the HLF reaction. Combining experimental techniques — laser flash photolysis (LFP), electron paramagnetic resonance (EPR), and nuclear magnetic resonance (NMR) — with computational density functional theory (DFT) calculations and kinetic modelling, we challenge the previous assumption that the HAT step was rate-limiting and regioselectivity was both under thermodynamic and kinetic control. We have identified that the halogen-atom transfer (XAT) step in the propagation cycle of the HLF reaction follows pseudo-first order kinetics and has the largest transition-state barrier. Additionally, we observed that regioselectivity is exclusively controlled by the intramolecular hydrogen atom transfer kinetics, while no thermodynamic preference exists in the formation of C_6- and C_5-chlorinated products. Our work predicts how to accelerate the HLF reaction and how we can control the regioselectivity by smarter selection of substrates based on calculations, which could provide better control of the reaction when implemented in organic synthesis.

KEYWORDS Propagation cycle, LFP, EPR, NMR, DFT calculations, kinetic modelling, rate-limiting step, regioselectivity, radical-mediated rearrangement, mechanistic study, hydrogen atom transfer (HAT), halogen atom transfer (XAT)

INTRODUCTION

The foundation for the use of N-centered aminyl radicals in organic synthesis, albeit not recognised as such, was laid more than a century ago. In 1881-1885, Hofmann[1] discovered that treating *N*-bromo-2-propylpiperidine, an *N*-halodialkylamine, with hot sulfuric acid produced a tertiary amine, eventually identified[2] as octahydroindolizine. Löffler and Freytag[3] extended the Hofmann reaction to simple secondary amines and discovered it to be a general approach for synthesising pyrrolidines.[4] Around 70 years after its discovery, Wawzonek and Helen,[5] followed by Corey and Hertler,[6] identified a free radical chain mechanism for this reaction. Upon the activation of *N*-chloroamine **1** with sulfuric acid (Scheme 1), the protonated *N*-chloroamine **2** undergoes homolytic cleavage in the presence of heat, light, or initiators. The resulted protonated aminyl radical **3** takes part in an intramolecular hydrogen atom transfer (HAT) abstracting a sterically favourably orientated hydrogen atom to afford, regioselectively, an alkyl radical **4**, which in turn abstracts a chlorine atom to form a chloroalkylammonium ion **5**, which then cyclises in the presence of a base providing cyclic tertiary amine **6**.

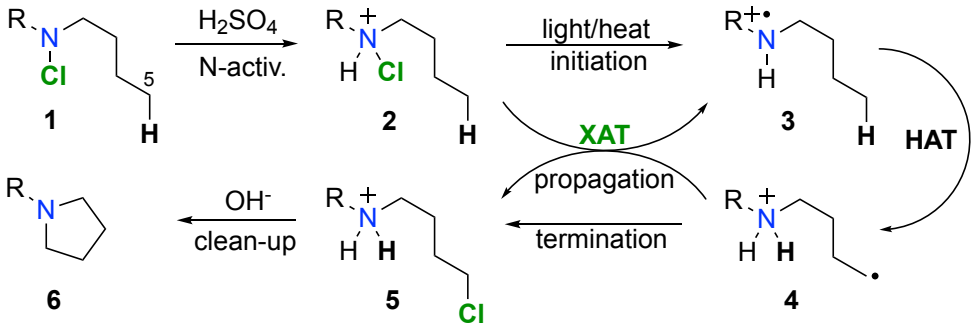

Scheme 1. Cyclization of N-Halogenated Amines (The Hofmann-Löffler-Freytag Reaction)[4]

There are two well-documented modern variants of the Hofmann-Löffler-Freytag Reaction (HLF), one developed by Suarez and coworkers,[7–10] who used *in situ* halogenation and photochemical activation of *N*-iodoamides to produce cyclisation products, and another reported by Corey et al.,[11]

where the required bromoamide precursor was synthesised and characterised in a separate first step. Subsequent irradiation of the bromoamide precursor in CCl_4 results in the formation of the C_5-bromo derivative, which can be cyclised to methyl 1-acetyl-3-methylpyrrolidine-2-carboxylate with a 90 % yield using a hindered base.

Mechanistic investigations, from the discovery of the HLF reaction until today, point conclusively to a radical chain mechanism involving intramolecular HAT as the first step of the propagation cycle, with halogen atom transfer (XAT) as the second step.[4,6,12–15] Intermolecular reactions involving neutral or protonated aminyl radicals have been documented, but only occur as additions to olefinic and acetylenic hydrocarbons and not as intermolecular HAT.[16–21] When olefins are present in the solvent, the intermolecular addition of protonated or neutral aminyl radicals to olefins competes with the intramolecular HAT step of the HLF propagation cycle depending on the reaction conditions.

To the best of our knowledge, few published studies have investigated the rate-limiting step of the HLF reaction and the inherent causes that guide regioselectivity. Wolff[4] has argued that the second step, XAT, has a smaller activation barrier and from this point on it was assumed that the HAT step is rate-limiting. In this context, extensive computational studies have been published investigating it,[22–25] where the thermodynamics of this step is evaluated *via* the radical stabilisation energies (RSEs) for a family of isodesmic reactions and plotted against corresponding activation barriers (Bell-Evans-Polanyi principle). The main conclusion from these studies is that the selectivity of attack by the aminyl radical on a carbon atom depends on the reactivity of the aminyl radical and on the stability of the ensuing carbon radical (see Figure 1). Therefore, aminyl radicals which can abstract hydrogen atoms from carbon generally show a preference for hydrogen in the order of tertiary > secondary > primary. Furthermore, by changing the activating group on the N-

centered aminyl radical, the outcome of the reaction can be dramatically influenced. This, however, does not provide an answer to whether the regioselectivity is determined by thermodynamics or kinetics and has not been placed in the context of the propagation cycle.

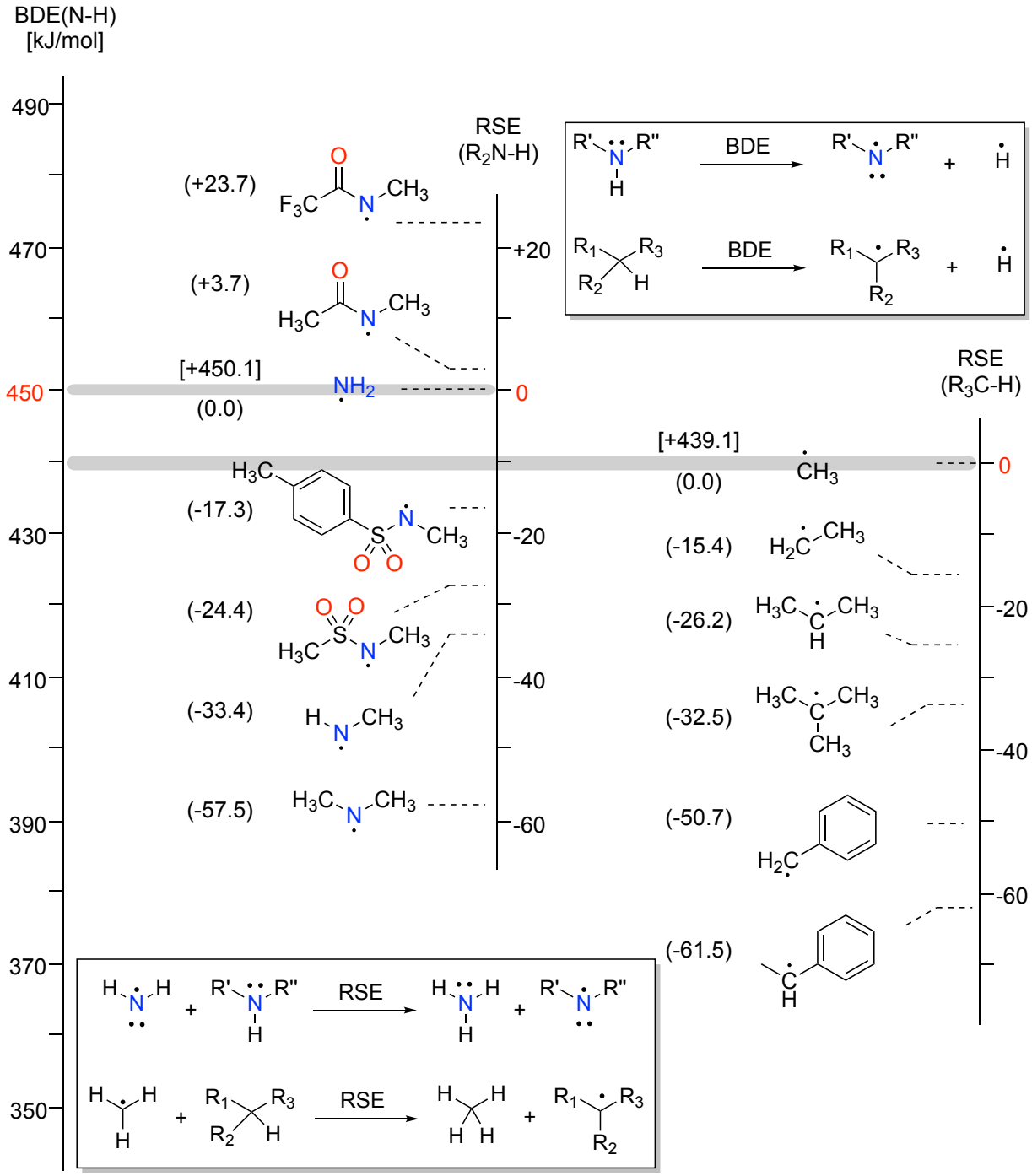

Figure 1. Bond dissociation energies (BDEs) and radical stabilization energies (RSEs) for selected small radical species commonly involved in HLF reactions. Grey bands denote anchor points between RSE and BDE scales. Data calculated at RO-B2PLYP/G3MP2large//B3LYP/6-31G(d) from references 16, 22 and 25.

The vast majority of papers dealing with HLF reaction report on pyrrolidine formation and there has been just one paper reporting on exclusive piperidine formation,[26] there have been, although, a couple of papers reporting on the functionalisation of the C_6 position with a chlorine atom.[27–29] To investigate the factors determining regioselectivity and identify the rate-limiting step, we have chosen a joint experimental and a computational approach to study a system that was employed in piperidine synthesis. Our aim is to detect as many as possible radical intermediate species involved in the propagation cycle and analyse major products formed. Quantum chemical calculations have been used extensively to identify these radical intermediates and reaction products. The proposed calculated reaction mechanism should explain experimental results, the observed regioselectivity and kinetic measurements. Finally, we propose that a combined approach involving both computational techniques and experiments must be employed when addressing fundamental questions, such as regioselectivity and the rate-limiting step of the reaction sequence must be answered.

RESULTS AND DISCUSSION

To provide experimental evidence for the interplay between two reaction steps in the propagation cycle, we employed NMR, LFP and EPR techniques (see Scheme 2). The overall reaction progress and major product analysis was observed with different NMR techniques, with *off-site* irradiation using a 370 nm Kessil lamp. Direct detection of radical intermediates with measurement of their

rearrangement kinetics was performed using LFP *via* the fourth harmonic of Nd_YAG laser (266 nm). Additionally, we attempted an *in-situ* generation and spin-trapping of N- and C-centered radicals using the phenylbutylnitrone (PBN) spin trap and investigated the resulting adducts with EPR (see Scheme 2c). Finally, we performed extensive DFT calculations and kinetic modelling of the reaction pathways, with the full model described in detail in subsection S12 of the Supporting Information.

a) NMR experiment

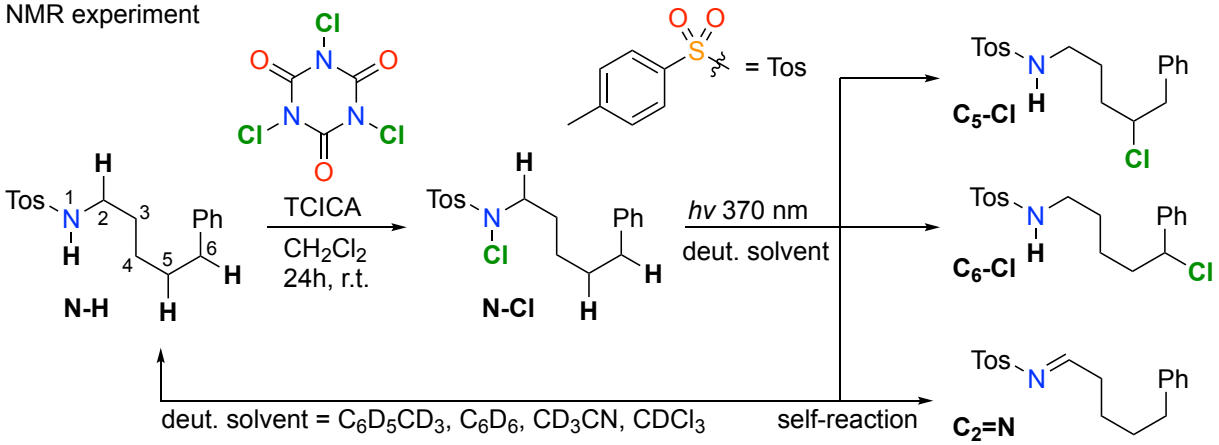

b) LFP experiment

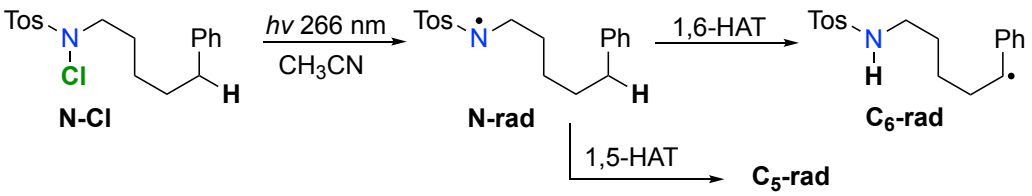

c) EPR experiment

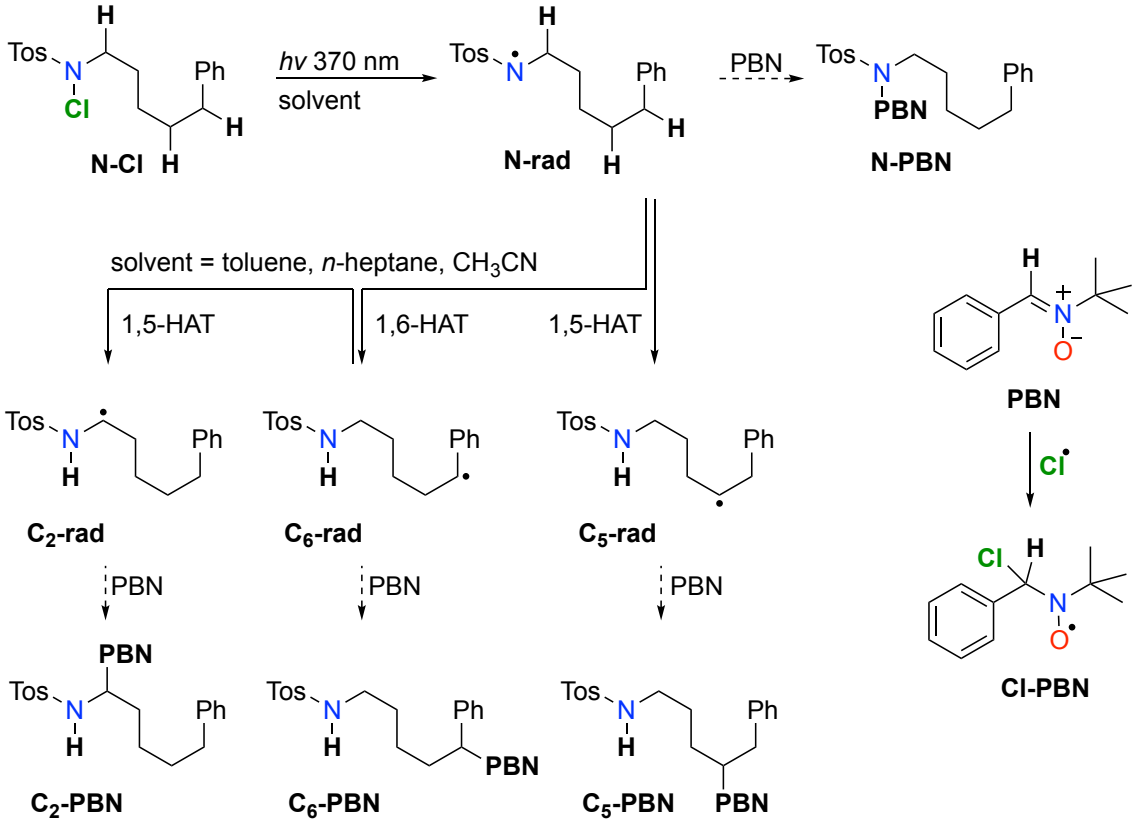

Scheme 2. Expected products and intermediates of HLF reaction were measured using three different techniques. (a) Synthesis of **N-Cl** and NMR observed products of the reaction mixture after 370 nm irradiation of **N-Cl**, (b) radical intermediates observed after laser excitation at 266 nm of **N-Cl** in flow cuvettes (3 mL; 3×10^{-4} M) at 266 nm in N_2-purged acetonitrile, (c) radical intermediates after 370 nm irradiation and PBN spin-trapped products in EPR experiment. Details of the experiments are found in the SI.

Using continuous irradiation with a UV lamp from the bottom of the cavity resonator, the complete reaction sequence was monitored with EPR spectrometry for **N-Cl** (Scheme 2c). The resulting experimental spectrum is shown in Figure 2. The best decomposition of the experimental EPR spectrum for **N-Cl** was found to be the one with one N-centered radical adduct, **N-PBN**, a Cl radical adduct, **Cl-PBN** and three C-centered radical adducts (assigned as **C_6-PBN**, **C_5-PBN** and **C_2-PBN**) with different hydrogen hyperfine couplings (*hfc*) (Table 1.). This total simulated spectrum, supported by our DFT calculations, aligns well with the experimental data (Figure 2.). As a result, we were able to observe a **Cl-PBN** adduct, proving homolytic cleavage of N–Cl bonds generating a chlorine radical that quickly combines with **PBN**. An **N-PBN** adduct was formed from the addition of N-centered radical to a **PBN** molecule. Calculated EPR parameters for **N-PBN** are in good agreement with experimental values. Finally, we were able to observe three distinct PBN adducts of C-centered radicals, namely **C_6-PBN**, **C_5-PBN** and **C_2-PBN**. Experimental *hfc* values of these three PBN adducts differ enough to distinguish them, although in DFT calculations, **C_6-PBN** and **C_5-PBN** have similar calculated *g*-factor values, while **C_2-PBN** differs from them. Calculated EPR parameters for **C_6-PBN** and **C_5-PBN** are in satisfactory agreement with experimental values. Difference in *g*-factors and *hfc* values of the **C_2-PBN** radical

adduct compared to the rest of C-centered radicals is due to different connectivity and closer secondary N-atom to the radical centre.[16] Again, calculated values for the **C_2-PBN** have the same trend as the experimental parameters. Additional support in correct assignment of radicals comes from similar experimental *g*-factors and *hfc* values for **C_2-PBN**, **N-PBN**, and **C5-PBN** radicals generated from N-chloro-N-hexyl-4-methylbenzenesulfonamide.[16] At this point it is worth noting the relative weights of the radical adducts are: **N-PBN** 1, **Cl-PBN** 0.72, **C_6-PBN** 0.12, **C_5-PBN** 0.17 and **C_2-PBN** 0.11.

Table 1. Experimental and calculated EPR parameters for observed radicals in the EPR spectrum. Calculated at B3LYP/(C,H,O)EPR-III/(S)def2-QZVP/(N)6-31G(d)//B3LYP/6-31G(d) level of theory. Hyperfine couplings (*hfc*) units are in Gauss.

	N-PBN		**Cl-PBN**	**C_6-PBN**		**C_5-PBN**		**C_2-PBN**	
	EXP	CALC	EXP	EXP	CALC	EXP	CALC	EXP	CALC
g	2.00612	2.0063	2.0077	2.0064	2.00591	2.0064	2.00599	2.0062	2.00611
α_N	13.82	14.21	12.37	13.96	14.78	13.96	15.32	13.72	14.06
α_H	2.85	3.87	0.76	3.06	3.67	2.03	2.37	7.38	5.49
$\alpha_{N'}$	1.54	1.57	α_{Cl} 6.23						
ratio	1.00		0.72	0.12		0.17		0.11	


C6-PBN
C5-PBN
C2-PBN
N-PBN
Cl-PBN
Sim
Exp
Exp
- N-PBN
Exp
- N-PBN
- Cl-PBN
Exp
- Sim
3480
3490
3500
3510
3520
3530

Figure 2. EPR spectra of spin-trapped radical intermediates generated with 370 nm irradiation of **N-Cl**. The simulated spectra of each radical adduct species are denoted on the spectra as **C_6-PBN**, **C_5-PBN, Cl-PBN**, **C_2-PBN**, and **N-PBN**. Total simulated spectrum is labelled as **Sim**, while experimental spectrum is labelled **Exp**, with residual signals provided as **Exp – N-PBN**, **Exp – N-PBN – Cl-PBN**, and **Exp – Sim**. Line widths measured with EPR and reaction yields were influenced by the effectiveness of air removal using freeze–pump–thaw cycles with backfill of argon or nitrogen gas. Experimental line widths of less than 0.4 G were deemed satisfactory for optimal resolution of radical adducts. More information on deconvolution and simulation is deposited in SI.

Before *off-site* irradiation, ^{1}H NMR and ^{13}C APT spectra of **N-Cl** (Scheme 2a) were recorded. All signals observed for the starting material are consistent with the expected ones for **N-Cl**. After *off-site* irradiation of the **N-Cl** precursor in toluene, a mixture of products was obtained with total conversion of starting material, as indicated by the ^{1}H NMR spectrum of the reaction mixture. Out of the total **N-Cl** compound in the NMR tube, ~42 % corresponds to the **N-H** product (Figure 3). The mechanism by which this reversal to the amine parent compound occurs has baffled us, although it is a common phenomenon reported in the literature.[18,28–30] Our first mechanism proposal involves the reaction of chlorine radical or N-centered radical **N-rad** with solvents,[20] producing solvent radicals and polymerization side reactions resulting in a cloudy reaction mixture.

The analysis of the other products using the ^{1}H NMR spectrum combined with the 2D technique, HSQC and ^{13}C APT spectra, provides unambiguous evidence that the signals observed at 4.47 and 3.75 ppm correspond to **C_6-Cl** and **C_5-Cl** products, respectively, with an overall NMR yield of ~47

% (**C_6-Cl** : **C_5-Cl** = 71 % : 29 %) (Figure 3). This was determined from the integral ratios (SI). From additional NMR experiments in other solvents, we found that approximately 50 % of **N-H** and 50 % of the **C_6-Cl** and **C_5-Cl** mixture (72 % : 28 %) were obtained in deuterated benzene. In deuterated acetonitrile, we obtained 66 % of **N-H** and 34 % of the **C_6-Cl** and **C_5-Cl** mixture (57 % : 43 %). We can safely conclude that the H-atom from the trace water is not involved in the mechanism of converting **N-Cl** back to the parent **N-H** species, due to the same pattern of product ratios in a wide selection of solvents. Alas, by examination we have observed a peak (δ 7.76, t, *J* = 11 Hz, in $CDCl_3$) in the aromatic NMR that corresponds to the imine signal, and NMR yield of ~11%. This indicates the occurrence of a self-reaction, facilitated by hydrogen atom transfer (HAT) between two **N-rad** molecules, leading to their termination and the formation of the starting amine (**N-H**) and imine (**C_2=N**) products. These disproportionation products are described in the literature,[31,32] and it is not a coincidence that many chemists deliberately design precursors with the C_2 position blocked or unavailable.[28–30] Additionally, the necessity of blocking the C_2 position in HLF reactions has been studied in detail in our previous work.[15] Our calculations predict a barrier of $\Delta G^{\ddagger}_{298}$ = +59.4 kJ mol^{-1}, with thermodynamic driving force of ΔG_{298} = −134.6 kJ mol^{-1} for this reaction.

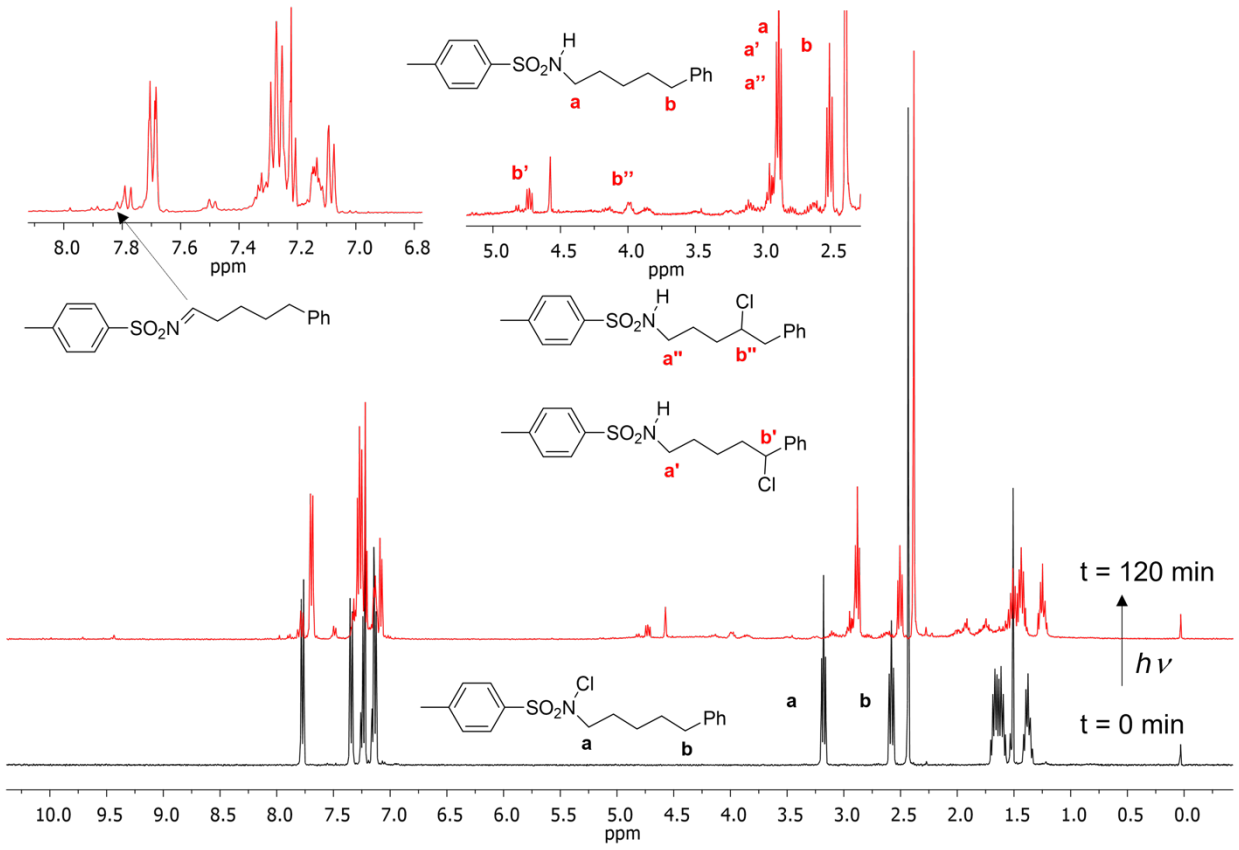

Figure 3. NMR spectra before and after *off-site* irradiation in $CDCl_3$. The black and red spectra correspond to the **N-Cl** and reaction mixture of **N-H**, **C_6-Cl**, **C_5-Cl**, and **C_2=N**, respectively. Insets depict selected signal ranges in more details, with chosen signals assigned. The ^{1}H, HSQC, and $^{13}C\{^1H\}$ APT spectra for experiments in C_6D_6 are deposited in SI.

LFP measurements were performed on an **N-Cl** in acetonitrile to directly detect the transient species generated after laser excitation at 266 nm (4.66 eV) (Scheme 2b). This resulted in the homolytic cleavage of the weakest N—Cl bond (4.03 eV)[33] and the formation of an aminyl radical and, through subsequent rearrangement reactions, corresponding C-centered radicals. This is

confirmed by EPR experiments in toluene, acetonitrile, and *n*-heptane, in which we detected **N-PBN** and **Cl-PBN** after irradiation of **N-Cl** (Figure 2).

The intramolecular HAT from one of the five carbon atoms of **N-Cl** to the nitrogen atom enables the formation of one or more C-centered radicals. Among these, a benzyl radical **C_6-rad**, is the most likely to be detected by LFP due to the benzene ring acting as a chromophore. The transient absorption spectrum (Figure 4) displays three distinct maxima: one at 280 nm, the second at 310 nm, and the third at 460 nm. The shape of these spectra does not change significantly within the 1500 ns timeframe after the laser excitation. However, it is understandable from the spectra that multiple transient species are present, which is deduced from the fact that some maxima disappear faster than others. Furthermore, there are no major changes in the shape of the spectra, which implies that the transient moieties are related and have major structural features in common. Conclusive evidence to support this comes from kinetic data collected at respective wavelengths. We have a first-order decay with two contributions at 290 nm and 330 nm. The shorter time scale at 290 nm better reflects the kinetics of the shorter-lived transient species, which lives less than 20 ns and is close to the detection limit, while the longer-lived transient determined from the extended time scale, has a lifetime (τ) of 25 μs at 290 nm and 47 μs at 330 nm. Kinetics at 450 nm follows the single exponential decay, with a τ similar to the longer component at 290 nm and 330 nm, 35 μs respectively. Small differences between the lifetime values may be due to variations in the signal-to-noise ratio (SNR), or due to different quantitative shares of the radicals presented (see SI). The shorter-lived transient at 290 nm is assigned to an aminyl radical formed by the N-Cl bond cleavage. Amidyl and aminyl radicals have previously been generated by LFP, and their τ have been reported, whether they were directly detected with LFP or indirectly from the detected C-

centered radical formed by cyclization/intramolecular HAT. Reported τ of amidyl and aminyl N-centered radicals range from 5 ns to 454 ns.[34–37] This is in agreement with our experimental results.

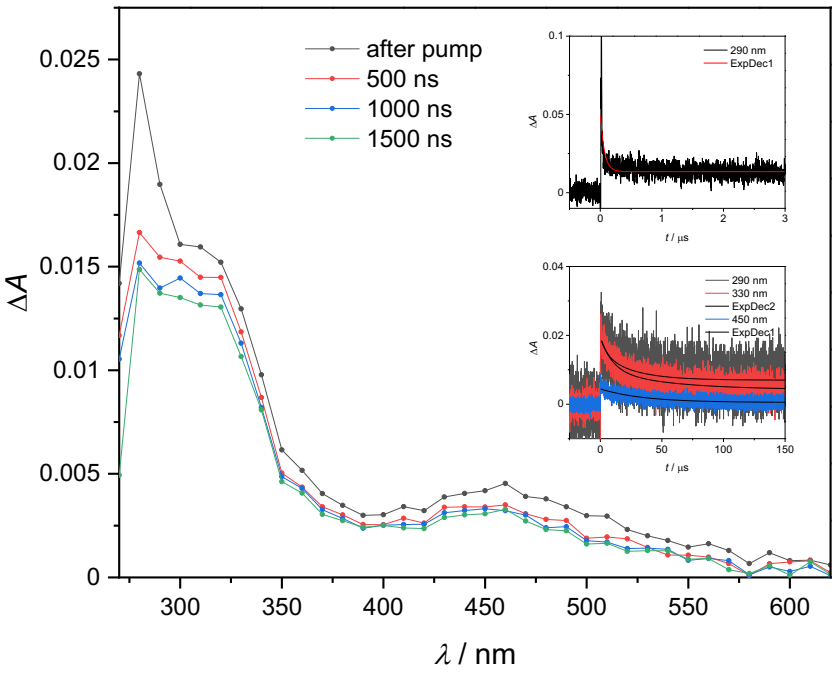

Figure 4. Transient absorption spectra of N_2 purged solution of 0.3 mM **N-Cl** in acetonitrile. Flow rate: 2.4 mL/min. E_{266} = 22 mJ. A_{266} = 0.27. Insets: Corresponding time profiles at 290 nm, 330 nm and 450 nm.

To check if the aminyl N-centered radical, **N-rad**, absorbs at 290 nm we have done extensive TD-DFT calculations that indicate a strong absorption peak at 280 nm with an oscillator strength (*f*) of 0.0238 (SI). We conclude that the longer-lived transient is one of the generated C-centered radicals, most likely a benzyl-type **C_6-rad**. This is in good agreement with the literature, which reports a lifetime of 40 µs for benzyl radicals, generated from benzyl chloride in hexane, with a

maximum at about 315 nm.[38] Additionally, our measurements of the benzyl radical generated from BnCl in acetonitrile show a maximum at 310 nm and a lifetime of 30 μs (S8 in SI).

As seen in Figure 5, DFT calculations of the 1,6-HAT step involves rearrangement from the global minimum on the reactant side (**N-rad$_{gm}$**) to a pre-reactive conformer (**N-rad$_{ric1,6}$**) that is ΔG_{298} = +25.3 kJ mol^{-1} less stable. From there, the transition state **TS-1,6-HAT$_{uni}$** is reached with an overall barrier of $\Delta G^{\ddagger}_{298,gm}$(**1,6-HAT$_{uni}$**) = +38.0 kJ mol^{-1}. When the barrier is defined as in eq. 1, $\Delta G^{\ddagger}_{298,ric}$(**1,6-HAT$_{uni}$**) equals 12.8 kJ mol^{-1}. In the first case ($\Delta G^{\ddagger}_{298,gm}$), the calculated $t_{1/2}$ of the aminyl radical is 514 ns, while for the second case ($\Delta G^{\ddagger}_{298,ric}$) the calculated $t_{1/2}$ of 0.02 ns is in far better agreement with LFP experimental results. This led us to the conclusion that upon homolytic cleavage (hc) of the N—Cl bond, the N-centered aminyl radical **N-rad$_{hc,pic}$** exists as a high energy conformer on the potential energy surface and is almost equal in energy to the pre-reactive conformer **N-rad$_{ric1,6}$** of the IRC path. This is a case when Boltzmann distribution does not apply, and the low energy state is unavailable due to kinetic reasons, with **N-rad$_{hc,pic}$** quickly rearranging to the **N-rad$_{ric1,6}$**. On the product side, the first local minimum encountered is **C6-rad$_{pic1,6}$** at ΔG_{298} = −35.9 kJ mol^{-1}, which then rearranges to the most stable conformer, a global minima (gm) **C6-rad$_{gm,uni}$** with an overall Gibbs free energy of reaction of ΔG_{298} = −57.0 kJ mol^{-1}. At this point, **C6-rad** and **N-Cl** species are separated in the solvent. When they meet in the solvent cage due to diffusion, a complex (**C6-rad—N-Cl**)$_{gm,bi}$ is formed at ΔG_{298} = −45.5 kJ mol^{-1} after which a pre-reactive conformer for the **XAT** is formed (**C6-rad—N-Cl**)$_{ric,XAT,bi}$ at ΔG_{298} = −43.4 kJ mol^{-1}. From there, the transition state **TS-1,6'-XAT$_{bi}$** is reached with an overall barrier of $\Delta G^{\ddagger}_{298,gm}$(**1,6'-XAT$_{bi}$**) = +52.1 kJ mol^{-1}. If the barrier is calculated according to eq 1. $\Delta G^{\ddagger}_{298,ric}$(**1,6'-XAT$_{bi}$**) value is at +38.5 kJ mol^{-1}. For the first case, the $t_{1/2}$ of the **C$_6$-rad** species

is 149 µs and for the second case the $t_{1/2}$ is 633 ns. The first case describes the $t_{1/2}$ of the radical **C_6-rad** closer to the experimental results.

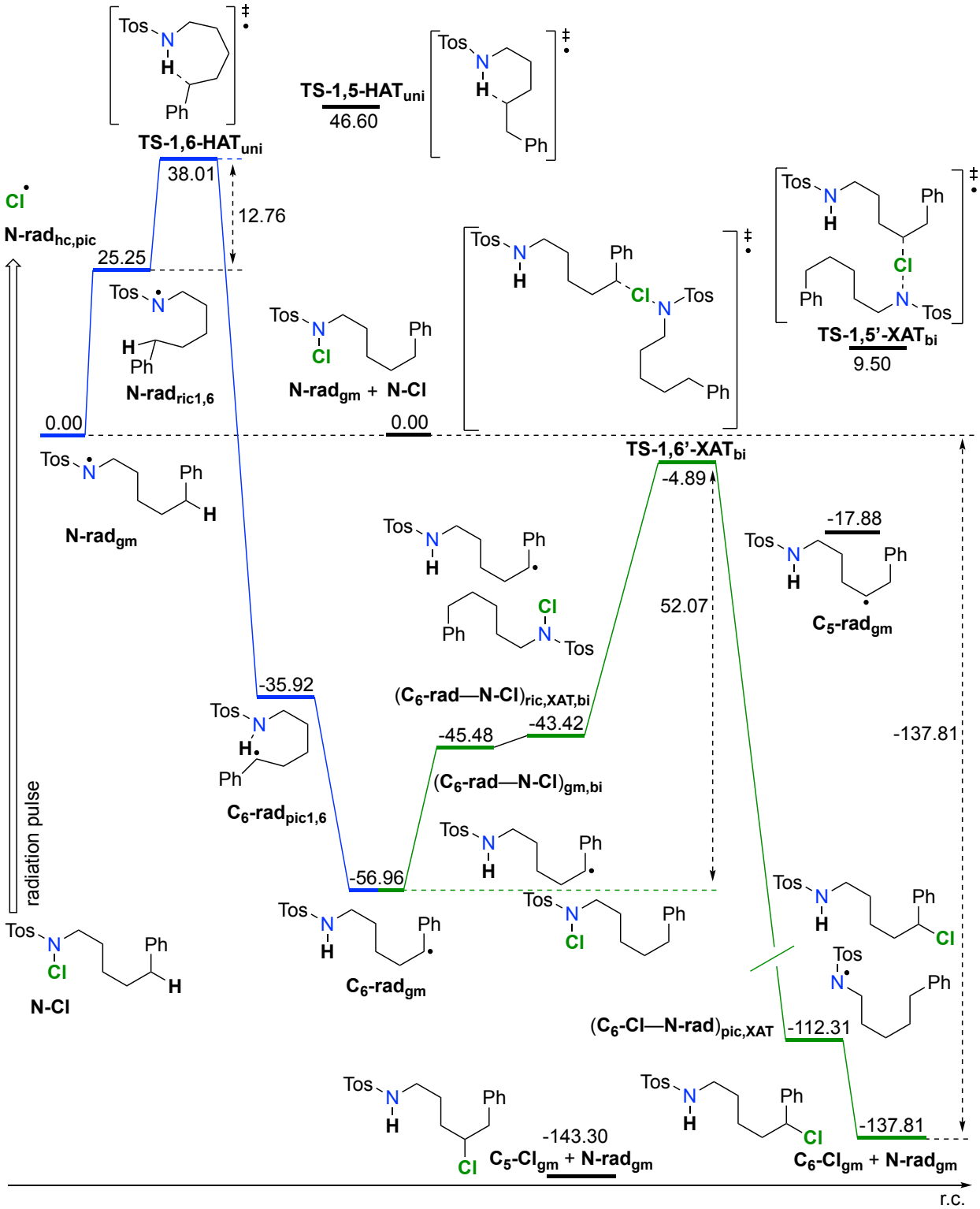

Figure 5. Energy diagram of intra- and intermolecular radical rearrangements for the propagation cycle of HLF for the 1,6-pathway. From the starting N-centered radical **N-rad**, it rearranges *via*

TS-1,6-HAT to the **C_6-rad**. The next step is the bimolecular reaction from **C_6-rad** and **N-Cl**, *via* **TS-1,6'-XAT**, to **C_6-Cl** and **N-rad** formation. Calculated at RO-B2PLYP/G3MP2Large(SMD,CH_3CN)//B3LYP/6-31G(d) level of theory. Included in the diagram are chosen points of the 1,5-pathway. Global minimum structure **N-rad$_{gm}$** is taken as a starting point in unimolecular process, while the global minima of separated reactants, namely **N-rad$_{gm}$** and **N-Cl$_{gm}$**, were taken as a starting point in bimolecular reaction. Units are in kJ mol^{-1}.

Hence, due to better fit with the experiment, we use $\Delta G^{\ddagger}_{298,ric}$**(1,6-HAT$_{uni}$)** calculated from the pre-reactive minimum for the HAT reaction as a first step in the propagation cycle, while for the second step, which involves a bimolecular XAT reaction, we use $\Delta G^{\ddagger}_{298,gm}$**(1,6'-XAT$_{bi}$)** again due to better fit to the experimental results.

We have also performed TD-DFT calculations that show that **C_6-rad** has an absorption peak at 295.36 nm with an oscillator strength of f = 0.0362 and that the N-centered aminyl radical, **N-rad**, has a strong absorption peak at 290 nm with an oscillator strength (f) of 0.0238 (SI). Our experimental lifetimes of the radicals in the LFP agree with the lifetimes reported in the literature sources and with the calculated data. This leads us to the conclusion that we have observed an N-centered aminyl radical and a benzylic-type **C_6-rad** in the LFP experiments.

As seen in Figure 2, there is a **C_2-rad** in the EPR spectra which can be formed *via* HAT from either **C_6-rad** (**1,5-HAT$_{CC,uni}$**) or from **N-rad** (**1,2'-HAT$_{bi}$**). A similar radical has been observed in the EPR spectra in the *N*-hexyl-4-methylbenzenesulfonamide system.[16] When compared to the other bimolecular HAT reactions (Figure 6), the barrier for the formation *via* **1,2'-HAT$_{bi}$** is between the barriers for the C-centered alkylic-type radical and benzyl-type radical. Thermodynamically, **C_2-rad** is the second most stable C-centered radical, with stability closer to the **C_6-rad**, than the **C_5-rad**. Calculated reaction energies for all these processes are slightly higher than the barriers

calculated in 1,6-pathway. This is especially true for the unimolecular HAT converting **C_6-rad** to the **C_2-rad**, with the highest calculated barrier of $\Delta G^{\ddagger}_{298}$ = +89.1 kJ mol^{-1}. However, the **C_2=N** imine species, product observed in the NMR experiment, is generated primarily by the self-reaction of two **N-rad** (see above), then from **C_2-rad**. Another pathway for imine production involves 1,2'-HAT transfer between **N-Cl** and **N-rad**, but this reaction is kinetically less favored with higher calculated barrier ($\Delta G^{\ddagger}_{298}$ = +79.53 kJ/mol).

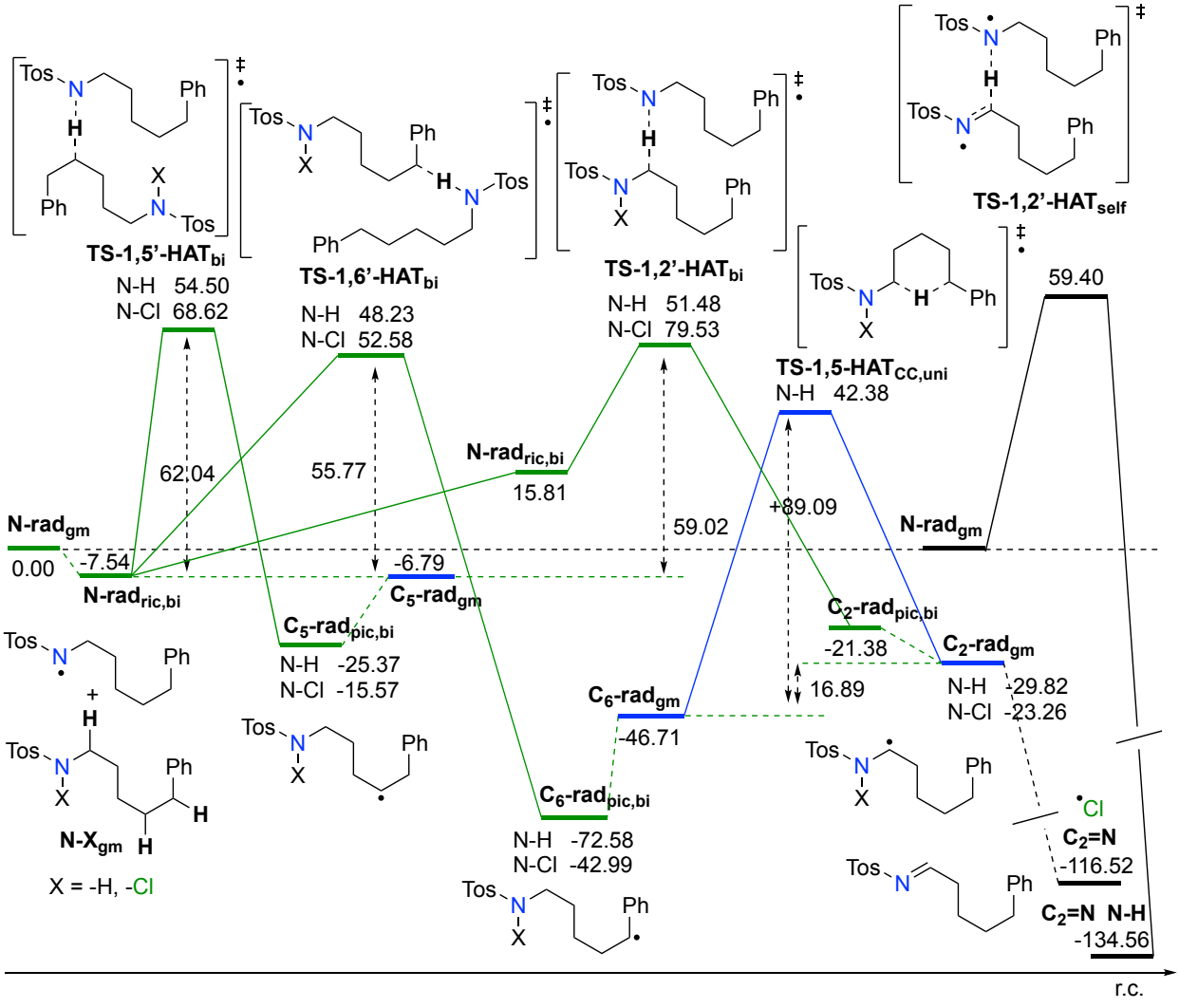

Figure 6. Energy diagram of intra- and intermolecular radical rearrangements to relevant C-centered radicals derived from **N-H** and **N-Cl**, and recombination through self reaction to **C2=N**

and **N-H** species. Calculated at RO-B2PLYP/G3MP2Large(SMD,CH_3CN)//B3LYP/6-31G(d) level of theory. Global minima of separated reactants, namely **N-rad$_{gm}$**, **N-Cl$_{gm}$** and **N-H$_{gm}$**, were taken as a starting point in the bimolecular reaction, while the global minimum structure on the reactant side, **N-rad$_{gm}$**, is taken as a starting point in the unimolecular process, and dimer of **N-rad$_{gm}$** is taken as the starting point for the self reaction. Units are in kJ mol^{-1}.

At this point, it is worth noting that the first-order decay kinetics shown in the insets of Figure 4, do not reach zero but form an onset close to zero. This implies that there is a steady state for a C-centered radical intermediate, which is presumably an intermediary species in the propagation cycle. Furthermore, the decay kinetics for **C$_6$-rad** can only be accurately described if the rate constant for the preceding elementary reaction is significantly larger or larger than the rate constant of the subsequent elementary reaction, assuming that these rate constants are the primary contributors to the observed experimental rate constants. This is corroborated by our DFT calculations as the calculated rate constant (eq 3.) for 1,6-HAT is 2.4×10^{10} s^{-1}, while for the bimolecular **XAT**, the rate constant is seven orders of magnitude lower, namely 4.63×10^{3} s^{-1}. Additionally, the lifetime of the N-centered aminyl radical **N-rad** is much shorter when compared to the lifetime of the C-centered radical **C$_6$-rad**. This is viable only when the second step is slower than the first. Thus, we conclude that the slow step of the propagation cycle is the intermolecular **XAT**. On the product side, the first local minimum encountered is **(C6-Cl—N-rad)$_{pic,XAT}$** at ΔG_{298} = −112.3 kJ mol^{-1}, which then rearranges to the most stable conformer **C6-Cl$_{gm}$** with an overall Gibbs free energy of reaction of $\Delta G_{298,rx,gm}$ = −137.8 kJ mol^{-1}.

For the 1,5-pathway (Figure 7), the HAT step involves rearrangement from the global minimum on the reactant side (**N-rad$_{gm}$**) to a pre-reactive conformer (**N-rad$_{ric1,5}$**) that is ΔG_{298} = +23.8 kJ

mol^{-1} less stable. From there, the transition state **TS-1,5-HAT$_{uni}$** is reached with an overall barrier of $\Delta G^{\ddagger}_{298}$ = +46.6 kJ mol^{-1}. When the barrier is defined from **N-rad$_{ric1,5}$** it amounts to only 22.8 kJ mol^{-1}, which includes a fast rearrangement step between high-energy conformer **N-rad$_{hc,pic}$** and **N-rad$_{ric1,5}$**. On the product side, the first local minimum encountered is **C$_5$-rad$_{pic}$** at ΔG_{298} = −1.9 kJ mol^{-1}, which then rearranges to the most stable conformer **C$_5$-rad$_{gm,uni}$** with an overall Gibbs free energy of reaction of ΔG_{298} = −17.9 kJ mol^{-1}. Species needed for the bimolecular reaction, namely **C5-rad** radical and **N-Cl** are still separated in the solvent. When they meet in the solvent cage due to diffusion, a complex (**C5-rad—N-Cl**)$_{gm,bi}$ is formed at ΔG_{298} = 1.9 kJ mol^{-1} which leads to a pre-reactive conformer of the **XAT** reaction (**C$_5$-rad—N-Cl**)$_{ric,XAT}$ at ΔG_{298} = 5.8 kJ mol^{-1}. From there, the transition state is reached with an overall barrier of $\Delta G^{\ddagger}_{298,gm}$(**1,5'-XAT$_{bi}$**)= +27.4 kJ mol^{-1}, while it amounts to $\Delta G^{\ddagger}_{298,ric}$(**1,5'-XAT$_{bi}$**) = 7.6 kJ mol^{-1} when the barrier is defined as in eq 1. On the product side, the first local minimum encountered is (**C$_5$-Cl—N-rad**)$_{pic,XAT}$ at ΔG_{298} = −137.2 kJ mol^{-1}, which then rearranges to the most stable conformer **C6-Cl$_{gm}$** with an overall Gibbs free energy of reaction of $\Delta G_{298,rx,gm}$ = −143.3 kJ mol^{-1}. To check if the **C$_5$-rad** radical moiety was detected in our LFP measurements at 290 nm we have done TD-DFT calculations that show that it has a strong absorption peak at 238.04 nm with an oscillator strength of f = 0.0290 (SI). This excludes the possibility for it to be detected in this experimental setup.

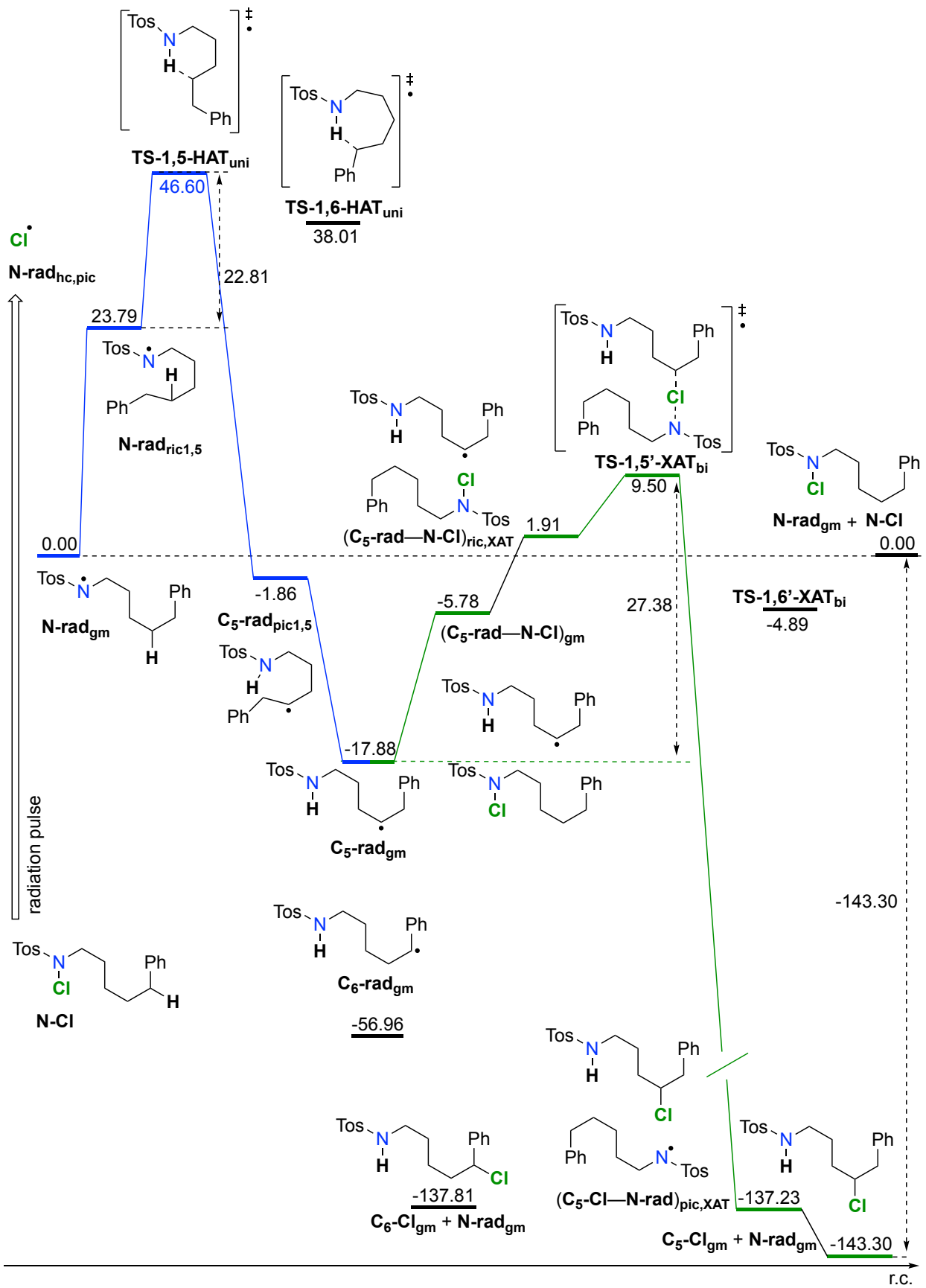
TS-1,5-HAT$_{uni}$
46.60
TS-1,6-HAT$_{uni}$
38.01
Cl•
N-rad$_{hc,pic}$
22.81
23.79
N-rad$_{ric1,5}$
0.00
N-rad$_{gm}$
-1.86
C$_5$-rad$_{pic1,5}$
(C$_5$-rad—N-Cl)$_{ric,XAT}$
1.91
TS-1,5'-XAT$_{bi}$
9.50
N-rad$_{gm}$ + N-Cl
0.00
TS-1,6'-XAT$_{bi}$
-4.89
-5.78
(C$_5$-rad—N-Cl)$_{gm}$
27.38
-17.88
C$_5$-rad$_{gm}$
radiation pulse
N-Cl
C$_6$-rad$_{gm}$
-56.96
-143.30
-137.81
C$_6$-Cl$_{gm}$ + N-rad$_{gm}$
(C$_5$-Cl—N-rad)$_{pic,XAT}$
-137.23
C$_5$-Cl$_{gm}$ + N-rad$_{gm}$
-143.30
r.c.

Figure 7. Energy diagram of intra- and intermolecular radical rearrangements for the propagation cycle of HLF for the 1,5-pathway. From the starting N-centered radical **N-rad**, it rearranges *via* **TS-1,5-HAT** to the **C_5-rad**. Next step is the bimolecular reaction from **C_5-rad** and **N-Cl**, *via* **TS-1,5'-XAT**, to **C_5-Cl** and **N-rad** formation. Calculated at RO-B2PLYP/G3MP2Large(SMD,CH_3CN)//B3LYP/6-31G(d) level of theory. Included in the diagram are chosen points of the 1,6-pathway. Global minimum structure on the reactant side, **N-rad_{gm}**, is taken as a starting point in unimolecular process, while the global minima of separated reactants, namely **N-rad_{gm}** and **N-Cl_{gm}**, were taken as a starting point in bimolecular reaction. Units are in kJ mol^{-1}.

The complete energy schemes (Figure 5 and Figure 7) for the 1,6- and 1,5-pathways allows us to compare similarities between the two processes. As observed, we notice that there is an early transition state for the second step and that the second step is irreversible, which in turn makes the whole cycle irreversible, even though the N-centered aminyl radical is regenerated. Furthermore, there is no thermodynamic preference for the formation of **C6-Cl** over **C5-Cl**, with both products in the same energy range (~ −140 kJ mol^{-1}), as compared to the starting **N-Cl** compound. The definition of the barrier from the global minimum, as in eq 2., describes experimental results much better for the second step, namely XAT-reaction, while the definition of the barrier from the pre-reactive minimum, as in eq 1., fits much better with the experimental results for the first step, namely HAT-step. Moreover, NMR analysis of the product mixture in toluene shows that we have 71.5 % **C_6-Cl** and 28.5 % **C_5-Cl**. This is an indication that the kinetics of the HAT step determine regioselectivity as the barrier for 1,6-HAT is 13.8 kJ mol^{-1} and for 1,5-HAT is 23.8 kJ mol^{-1}. When Bodenstein approximation of quasi-stationary behaviour[39,40] and the long chain approximation are applied to radical chain reactions, the reaction rates of the individual steps in

the cycle are equal. However, different rate constants strongly imply the quite large steady-state concentration of the C-centered radicals, **C_5-rad** and **C_6-rad**, each in its own cycle, compared to the **N-rad** created in the propagation step. When these approximations are applied in our kinetic model, we obtained that the HLF reaction follows pseudo first order kinetics with respect to the second step. Thus, we propose that the rate of the propagation cycle of the HLF reaction is controlled by the XAT step, which is additionally supported by both the LFP experiments and DFT calculations.

There is another interpretation of the reaction sequence in the literature, which was proposed by Muñiz for the selective synthesis of piperidines.[24] Instead of uni-(intra-)molecular HAT, they considered a bi-(inter-)molecular HAT, where N-centered succinimide radical extracts selectively only the C_6-H, providing the C-centered benzylic radical. Since there is no outside chlorinating agent in our reaction (halogenation was performed in the previous reaction step and quantitively removed), the only possible **1,6'-HAT_{bi}** is the reaction of **N-rad** with **N-Cl**, where the hydrogen extraction comes from the N-Cl species. The calculated barrier is $\Delta G^{\ddagger}_{298,ric}$(**1,6'-$HAT_{bi}$**)= +52.6 kJ mol^{-1}, which corresponds to $t_{1/2}$ of 8.73 ms for the **N-Cl-C_6-rad** specie. Similar results, $\Delta G^{\ddagger}_{298,ric}$(**1,5'-$HAT_{bi}$**) = +68.62 kJ mol^{-1} and $t_{1/2}$ of 98.28 ms is obtained for the 1,5-pathway (see Fig. 6). This is in stark contrast to the experimental values obtained from the LFP experiments, where degradation is much quicker. Products of these reactions, **N-Cl-C_6-rad** and **N-Cl-C_5-rad** are lower in energy, with thermodynamic driving force of –43.0 kJ mol^{-1} and –15.6 kJ mol^{-1}, respectively. As discussed above, **C_2-rad** is also a good candidate for the HAT reaction.[16] Yet this radical or downstream products (imine and **C_2-Cl**) were not observed in the Muñiz synthesis,[24] which is another reason why this reaction should be re-examined. After the C-centered radical formation, a uni-(intra-)molecular XAT process can envisioned as the final step in the reaction

sequence. It should be noted that Muñiz and coworkers make this a bimolecular XAT process with their halogen source (N-bromo-succinimide complex with I_2). For the unimolecular TS-1,6-XAT, from **N-Cl-C$_6$-rad$_{ric}$** structure, the kinetic barrier is $\Delta G^{\ddagger}_{298,ric}$(**1,6-XAT$_{uni}$**) = +101.9 kJ mol^{-1}, due to a very extended structure. Thermodynamics of this reaction is exergonic, with post-reactive intermediate complex **N-rad-C$_6$-Cl$_{pic}$** being –70.5 kJ mol^{-1}. For the similar unimolecular TS-1,5-XAT, the reaction barrier is lower ($\Delta G^{\ddagger}_{298,ric}$(**1,5-XAT$_{uni}$**) = +75.1 kJ mol^{-1}), with thermodynamic of this step comparable to the 1,6-XAT. It should be noted that the starting points for both **XAT$_{uni}$** processes, namely **N-Cl-C$_6$-rad$_{ric}$** and **N-Cl-C$_5$-rad$_{ric}$** have a 50.4 kJ mol^{-1} difference in energy, with benzyl-type of C-radical more stable than alkyl-type of C-radical. In conclusion, pathways with bimolecular HAT and unimolecular XAT are unfavourable, and thus should be excluded as possible mechanisms of the propagation cycle.

To support our experimental and computational results, we have done kinetic modelling of the HLF reactions in the case when only one major product is formed in a yield greater than 99 %. In our kinetic modelling, we applied a steady-state approximation for the concentration of the N radical, which we consider reasonable since the N radical is continuously consumed and regenerated throughout the reaction cycle (S12 in SI). This approximation also indirectly implies steady states for the **C$_5$-rad** and **C$_6$-rad** intermediates, as their concentrations are tied to the steady state behaviour of **N-rad**, through the dominant **C$_6$-Cl** pathway. Additionally, the reverse reactions in the second step of each pathway (reactions from chlorinated products **C$_5$-Cl**, **C$_6$-Cl**, and **C$_2$-Cl** back to their respective radicals and **N-Cl**) were neglected. This is supported by Gibbs energy profiles (Figures 5, 6 and 7), which indicate significantly higher energy barriers for these reverse reactions. As a result, they are unlikely to contribute significantly to the overall kinetics. Using the

approximations, we derived a simplified equation that describes the formation of all (final) chlorinated products, as presented in eq 4.

$$\mathbf{C_6\text{-}rad} + \mathbf{N\text{-}Cl} \underset{k_{5r}}{\overset{k_{5f}}{\rightleftharpoons}} \mathbf{C_6\text{-}Cl} + \mathbf{N\text{-}rad}$$

$$[\text{product}](t) = c_{\max}(\text{product})\left(1 - e^{-k_{5f}[C6]_0 t}\right) \qquad \text{(eq4)}$$

Here c_{max} represents the maximum concentration of the product, while k_{5f} and k_{5r} denote forward and reverse rate constants, respectively. Full derivation is presented in the SI. The exponent $-k_{5f}[C_6]_0$ applies to all products as **N-Cl** depletion is predominantly controlled by the **C6-Cl** pathway. As this pathway dictates the overall reaction kinetics, the time-dependent behaviour of all products follows the same exponential decay. This pseudo-first-order approximation is in good accordance with the experimental data from the LFP measurements. In addition, we also estimated the reaction half-lives and product ratios, which support the model's consistency and generally align with the experimental data (S12 in SI).

Understanding that XAT is the bottleneck step in the HLF reaction is crucial for controlling the reaction kinetics, predicting the duration of each step and the overall process, and designing specific termination steps.[69] Formed carbon-centered radicals can react with common halogenating agents in a one-pot reaction setup, such as trichloroisocyanuric acid (TCICA), *N*-chlorosuccinimide (NCS), *N*-bromosuccinimide (NBS), *N*-iodosuccinimide (NIS), or even iodine/sodium iodide (I_2/NaI), with lower or negligible activation barriers, leading to functionalised sp^3-hybridised carbon centers. This pathway bypasses the propagation step, where nitrogen-centered radicals are converted to carbon-centered radicals that promptly terminate with the halogen source. New nitrogen-centered radicals must then be generated *via* irradiation, which

can occur under one-pot reaction conditions where N-halogenation happens simultaneously with the HLF reaction.

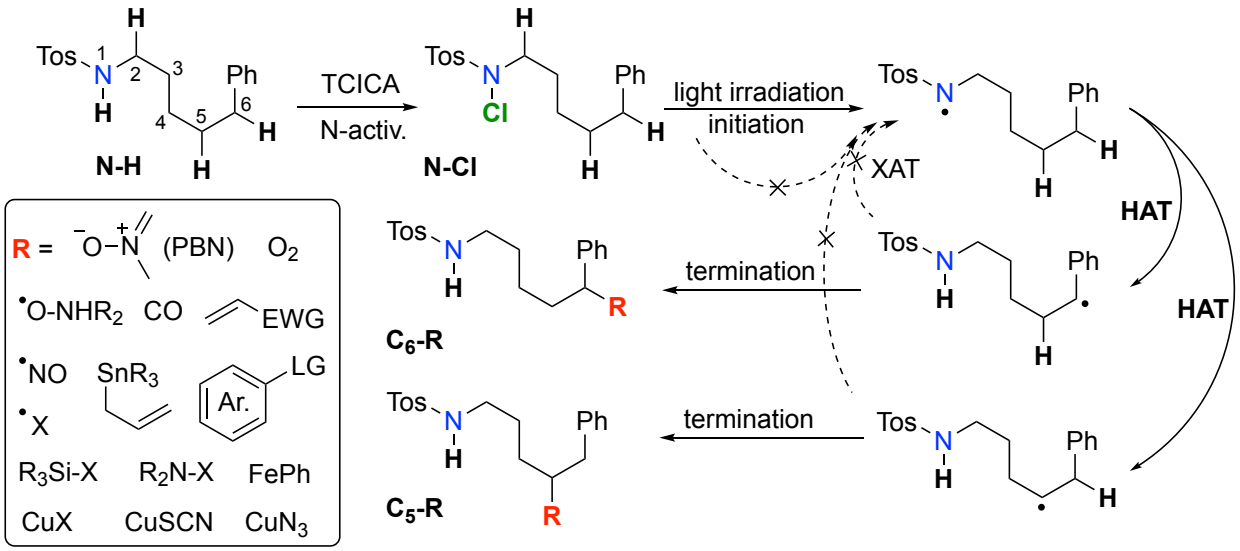

Scheme 3. Propagation *vs*. termination step in the HLF reactions. Different selection of termination traps may compete with XAT and the closing of the propagation site.

Moreover, this mechanism opens possibilities for remote δ- and ε-site functionalisation if suitable targets for radical addition are present. For such transformations to occur, the termination reaction must be both faster than the XAT step and thermodynamically more favourable than the halogenated products. An example is the reaction of carbon-centered radicals with a PBN spin trap, yielding an extremely stable NO-type radical in our EPR experiments. Other potential reactions can involve weakly bonded main group molecules (N–X, Si–X, Sn–H, Sn–allyl), metal salts (CuX, CuSCN, CuN_3), and π-systems (alkenes, arenes). We are currently exploring these possibilities in our laboratory and encourage other researchers to investigate these avenues, as they may lead to novel strategies in radical chemistry and synthetic methodologies.

CONCLUSIONS

Using NMR spectroscopy, laser flash photolysis LFP, and EPR spectroscopy in combination with DFT calculations and kinetic modelling, we monitored the reaction profile and identified significant intermediate radicals and products in the Hofmann–Löffler–Freytag reaction (HLF). Our results indicate that there is no thermodynamic preference for the formation of **C_6-Cl** over **C_5-Cl**, and the difference in ratios (72% *vs* 28%, respectively) is due to the **C_6-Cl** being a kinetic product. Thus, the kinetics of the HAT step in the propagation cycle guides the regioselectivity of the HLF reaction, and by calculating the barrier for the HAT step we can predict the major product formed. Moreover, we deduce that the slow step of the HLF reaction is the bimolecular XAT step. Additionally, we propose that adding halogen sources, typically used as chlorinating agents, or other traps may interfere with the XAT step of the propagation cycle, promoting earlier termination of a reaction cycle. We recommend that future research on radical mechanisms be conducted using a combination of experimental techniques paired with rigorous quantum-chemical calculations and kinetic modelling for a comprehensive overview of the reaction.

MATERIALS AND METHODS

The purchased compounds were sourced from Sigma-Aldrich (St. Louis, MO, USA) (trichloroisocyanuric acid (TCICA), Celite® S, hydrochloric acid (37%), acetone, silicone oil, petroleum ether, and cyclohexane), Fisher Scientific (Waltham, MA, USA) (toluene (anhydrous), acetonitrile (anhydrous), 1,4-dioxane (anhydrous), tetrahydrofuran (anhydrous), *N*,*N*-dimethylformamide (anhydrous), *N*,*N*-dimethylacetamide, 1,2-dichloroethane (anhydrous), and dichloromethane (anhydrous), dichloromethane (CH_2Cl_2)) and Kemika (Zagreb, Croatia) (sodium hydroxide). All reagents and chemicals were obtained commercially and used without further

purification unless otherwise noted. The starting material, 4-methyl-*N*-(5-phenylpentyl)benzenesulfonamide, **N-H**, was provided by the research group of Prof. Hendrik Zipse from Ludwig-Maximilian University, Munich, Germany, and ^{1}H and $^{13}C\{^{1}H\}$ NMR spectra values of the compound (see SI) correspond to the previously reported values.[26]

Chromatographic purification of the products was carried out using column chromatography filled with silica gel (Macherey-Nagel) 0.063–0.2 mm, and appropriate solvent mixtures of petroleum ether/ethyl acetate were used as eluents. Thin-layer chromatography (TLC) was performed on precoated TLC plates ALUGRAM SIL G/UV254, 0.20 mm silica gel 60 with a fluorescent indicator UV254 (Macherey-Nagel) in the appropriate solvent system. TLC spots were observed *via* the illumination with UV light at a wavelength of 254 nm after the immersion of the plate in an aqueous solution of $KMnO_4$ (3 g $KMnO_4$, 20 g K_2CO_3, 5 mL aq. NaOH 5 %, and 300 mL water) followed by heating. If TLC spots were not visible after illumination with UV light, they were detected utilizing an iodine chamber.

NMR spectra of the reaction mixture were obtained on a Varian Inova 400 NMR spectrometer operating at 399.90 MHz for ^{1}H NMR and 100.6 MHz for ^{13}C NMR and are reported as chemical shifts (δ) in ppm. The spectra were imported and processed in the MestreNova 11.0.4 program.[41]

EPR spectroscopy was performed using a Bruker ELEXSYS E500 EPR spectrometer with an ER4122SHQE cavity resonator. As this cavity resonator does not have an optical window for illumination, the light source was mounted underneath the cavity, with light coming through the bottom of the EPR 4 mm inner-diameter tube. EPR deconvolution and simulation were done using an EasySpin module with the MATLAB program package.[42] EPR visualisation and spectroscopy were done using the VisualEPR Web page.[43] For experiments, 35 mg of **N-Cl** was dissolved in the

0.3 mL of solvent (~0.04 M), degassed, and then mixed with degassed 10 mg of **PBN** dissolved in 0.3 mL of the same solvent (~0.015 M).

Transient absorption spectroscopy (TAS) measurements were performed using a nanosecond laser flash photolysis setup. The setup consists of a Nd:YAG laser (Quantel, Q-smart 450) and an LP980 transient absorption spectrometer (Edinburgh Instruments). The ground state absorption of the samples was adjusted to 0.3 at the 266 nm laser excitation wavelength (5 ns pulse duration, 10 Hz). The laser pulse energy at 266 nm was in the range of 10–23 mJ (30–70 mJ cm^{-2}). Kinetic measurements were performed in 1 cm quartz cells sealed with rubber septa. The transient absorption spectra were measured in a flow cell, with a flow rate set to 2.4 mL/min to ensure that no light was absorbed by the photoproducts. All solutions were prepared immediately before the experiments. Solutions were purged with high-purity N_2 for 20 min prior to the kinetics measurements and for 1 h before spectra measurements. All measurements were performed at 25 °C. UV–Vis spectra of the sample solutions were recorded using a Varian Cary 4000 spectrophotometer (Figures S1-S2).

The conformational space for all the local minima and saddle points of the 1st order on the energy diagram was investigated using the Conformer–Rotamer Ensemble Sampling Tool─CREST[44]coupled with the xtb-GFN2 program package and meta-dynamics simulation using xtb-GFN1[45] and xtb-GFN2.[46] The obtained structures were reoptimised using the B3LYP/6-31G(d) level of theory.[47–49] For each structure with a stable wave function, frequency calculation was performed to identify the minima and transition-state structures. Lowest lying conformers, e.g. with the lowest energy value for each species were labelled global minima (gm) on potential energy surface (PES). Transition state structures were differentiated from the minima as having exactly one imaginary frequency. From all transition state conformers, an intrinsic reaction

coordinate (IRC) search was performed to characterise the corresponding reaction/product channel, the last point in the forward and reverse direction was then optimised to the nearest local minimum i.e. reactive complex. On the reactant side, the obtained structure was termed pre-reactive intermediate complex (ric), while on the product side, the optimised structure was named post-reactive intermediate complex (pic). Single point energies were obtained with universal continuum solvation model SMD,[50] with acetonitrile as a solvent and RO-B2PLYP[52,53] with a G3MP2 large basis set[54] on geometries obtained at the B3LYP/6-31G(d) level of theory, with additional D3 dispersion correction.[55] The thermal corrections to the free energy were derived from the frequency calculations under the conditions of 298.15 K and 1 atm. The activation free energies ($\Delta G^{\ddagger}_{298}$) of each elementary reaction are defined in two distinct ways namely through equations:

$$\Delta G^{\ddagger}_{298,\mathrm{ric}} = G(\text{transition state}) - G(\text{reactant complex}) \quad (1)$$

$$\Delta G^{\ddagger}_{298,\mathrm{gm}} = G(\text{transition state}) - G(\text{global minimum}) \quad (2)$$

According to transition state theory (TST)[56,57], approximate reaction rate constants for elementary reactions, in which the reactants directly generate products, were estimated based on the Eyring-Polanyi equation as eq. (3):

$$k_{calc} = \frac{k_{\mathrm{B}}T}{h} e^{\frac{-\Delta G^{\neq}}{RT}} \quad (3)$$

where k_{B} is the Boltzmann constant, T is the temperature, h is Planck's constant, R is the molar gas constant, and $\Delta G^{\ddagger}$ is the activation free energy.

Calculations of EPR parameters were done using the B3LYP functional and a mixed basis set: EPR-III for C, H, and O atoms, def2-QZVP for the S atom, and 6-31G(d) for the N atom. A small basis set on the N atom is necessary for the correct calculations of the *g*-factor and hyperfine constants (*hfc*).[58,59] When using a larger basis set for the N atom, e.g., EPR-III or def2-QZVP, the obtained results systematically underestimate the *hfc*. Calculations were performed on the

Gaussian version 16.C01[60] using the advanced computing service (clusters Isabella and Supek) provided by the University of Zagreb University Computing Centre—SRCE[61] and the computational resources of the PharmInova project (sw.pharma.hr) at the University of Zagreb Faculty of Pharmacy and Biochemistry.[62]

Electronic transition spectra were calculated at the gas phase and in acetonitrile with Time Dependent[63] CAM-B3LYP[64]/TZVP/PCM[51] method at the molecular geometries optimised at B3LYP/TZVP level.

In order to account for the entropic effect of the presence of solvent molecules around a solute, the cell model presented by Ardura et al. was used.[65] This model is proposed in order to explicitly evaluate the effect of the loss of translation degrees of freedom in solution on the Gibbs activation energy in a bimolecular (or higher order of molecularity) reaction.[66]

We performed kinetic modelling of the reaction pathways, with the full model described in detail in subsection S12 of the Supporting Information. The complete mathematical model, which incorporates all possible reaction steps, leads to a system of nonlinear differential equations that is exceedingly complex and likely impossible to solve analytically due to the nonlinearity and the interdependence of the species' concentrations.[67–70] Numerical methods like Runge-Kutta could be applied; however, the potential solution may be highly sensitive to the initial conditions, particularly to the concentration of radicals formed after the laser pulse.[71,72] In such calculations, the uncertainty in starting conditions may induce numerical instability.[69,73,74] Therefore, some necessary approximations were applied to reduce the complexity of the model.

ASSOCIATED CONTENT:

• Data Availability Statement

The data underlying this study are available in the published article and its Supporting Information.

• Supporting Information Statement

Supporting information with experimental details, synthesis procedure, reactant, and product characterisation, EPR simulation parameters, calculation procedures, geometries and energies of optimised structures, and recorded NMR and EPR spectra are provided. The following files are available free of charge. SI.pdf (file type PDF)

AUTHOR CONTRIBUTION

G.Z. conceived the idea for this work; G.Z. and D.Š. did computational work; K.P. and T.P. purified and prepared chemicals and respective solvents; L.A. and I.Dž. carried out the LFP experiments and data processing; E.B. and J.Y. did EPR studies; V.V. was responsible for NMR measurement and analysis; kinetic modelling was done by T.F. Supervision was provided by E.B., V.V., and D.Š.; G.Z. and D.Š. wrote the manuscript with input from all authors. All authors participated in discussion and revision of the manuscript.

AUTHOR INFORMATION

The authors declare no competing financial interests.

ACKNOWLEDGMENT

Authors would like to acknowledge financial support from Croatian Science Foundation Installation Grant UIP-2020-02-4857 LIGHT-N-RING, Research Grant IP-2022-10-2634 Pharma-Eco, and computational resources provided by Advanced computing service on Cluster Supek, EU funded through KK.01.1.1.08.0001, at University of Zagreb University Computing Centre –

SRCE. Support from The Cryogenic Centre at the Institute of Physics (project KaCIF, KK.01.1.1.02.0012) is acknowledged. This work was also supported by the project FarmInova, (KK.01.1.1.02.0021) funded by the European Regional Development Fund, and Croatian Science Foundation Research Grant IP-2019-04-8846. Authors would like to thank Prof. Hendrik Zipse and Dr. Salavat Ashirbaev from Ludwig-Maximilian University for collaboration, and Assoc. prof. Boris Maryasin for fruitful discussions.

REFERENCES

(1) Hofmann, A. W. Ueber die Einwirkung des Broms in alkalischer Lösung auf Amide. *Ber. Dtsch. Chem. Ges.* **1881**, *14* (2), 2725–2736. https://doi.org/10.1002/cber.188101402242.
(2) Hofmann, A. W. Ueber die Einwirkung des Broms in alkalischer Lösung auf die Amine. *Ber. Dtsch. Chem. Ges.* **1883**, *16* (1), 558–560. https://doi.org/10.1002/cber.188301601120.
(3) Hofmann, A. W. Zur Kenntniss der Coniin-Gruppe. *Ber. Dtsch. Chem. Ges.* **1885**, *18* (1), 109–131. https://doi.org/10.1002/cber.18850180126.
(4) Löffler, K.; Kober, S. Über die Bildung desi-Nicotins ausN-Methyl-p-pyridyl-butylamin (Dihydrometanicotin). *Ber. Dtsch. Chem. Ges.* **1909**, *42* (3), 3431–3438. https://doi.org/10.1002/cber.19090420378.
(5) Wolff, M. E. *Cyclization of N-Halogenated Amines (The Hofmann-Löffler Reaction).* ACS Publications. https://doi.org/10.1021/cr60221a004.
(6) Wawzonek, S.; Thelen, P. J. Preparation of N-Methylgranatanine. *J. Am. Chem. Soc.* **1950**, *72* (5), 2118–2120. https://doi.org/10.1021/ja01161a068.
(7) Corey, E. J.; Hertler, W. R. A Study of the Formation of Haloamines and Cyclic Amines by the Free Radical Chain Decomposition of N-Haloammonium Ions (Hofmann-Löffler Reaction) [1]. *J. Am. Chem. Soc.* **1960**, *82* (7), 1657–1668. https://doi.org/10.1021/ja01492a035.
(8) de Armas, P.; Francisco, C. G.; Hernandez, R.; Salazar, J. A. Steroidal N-Nitroarnines. Part 4.'Intramolecular Functionalization of N - Nitroamine Radicals: Synthesis of I ,4-Nitroimine Compounds. **1988**, 11.
(9) Dorta, R. L.; Francisco, C. G. Hypervalent Organoiodine Reagents in the Transannular Functionalisation of Medium-Sized Lactams: Synthesis of I-Azabicyclo Compounds. 2.
(10) Carrau, R.; Hernández, R.; Suárez, E.; Betancor, C. Intramolecular Functionalization of N-Cyanamide Radicals: Synthesis of 1,4-and 1,5-N-Cyanoepimino Compounds. *J. Chem. Soc., Perkin Trans. 1* **1987**, No. 0, 937–943. https://doi.org/10.1039/P19870000937.
(11) Hernández, R.; Medina, M. C.; Salazar, J. A.; Suárez, E.; Prangé, T. Intramolecular Functionalization of Amides Leading to Lactams. *Tetrahedron Letters* **1987**, *28* (22), 2533–2536. https://doi.org/10.1016/S0040-4039(00)95460-1.
(12) Reddy, L. R.; Reddy, B. V. S.; Corey, E. J. Efficient Method for Selective Introduction of Substituents as C(5) of Isoleucine and Other α-Amino Acids. *Org. Lett.* **2006**, *8* (13), 2819–2821. https://doi.org/10.1021/ol060952v.

(13) Corey, E. J.; Hertler, W. R. A Study of the Formation of Haloamines and Cyclic Amines by the Free Radical Chain Decomposition of N-Haloammonium Ions (Hofmann-Löffler Reaction) [1]. *J. Am. Chem. Soc.* **1960**, *82* (7), 1657–1668. https://doi.org/10.1021/ja01492a035.

(14) Minisci, F. Free-Radical Additions to Olefins in the Presence of Redox Systems. *Acc. Chem. Res.* **1975**, *8* (5), 165–171. https://doi.org/10.1021/ar50089a004.

(15) Wawzonek, S.; Nelson, M. F.; Thelen, P. J. Preparation of Quinuclidines [1]. *J. Am. Chem. Soc.* **1951**, *73* (6), 2806–2808. https://doi.org/10.1021/ja01150a111.

(16) Zubčić, G.; You, J.; Zott, F. L.; Ashirbaev, S. S.; Kolympadi Marković, M.; Bešić, E.; Vrček, V.; Zipse, H.; Šakić, D. Regioselective Rearrangement of Nitrogen- and Carbon-Centered Radical Intermediates in the Hofmann–Löffler–Freytag Reaction. *J. Phys. Chem. A* **2024**, *128* (13), 2574–2583. https://doi.org/10.1021/acs.jpca.3c07892.

(17) Neale, R. The Chemistry of Nitrogen Radicals. V. The Free-Radical Addition of Dialkyl-N-Chloramines to Olefinic and Acetylenic Hydrocarbons.

(18) Neale, R. S.; Hinman, R. L. The Chemistry of Ion Radicals. The Free Radical Addition of N-Chlorodialkylamines to Butadiene. *J. Am. Chem. Soc.* **1963**, *85* (17), 2666–2667. https://doi.org/10.1021/ja00900a033.

(19) Neale, R. S.; Marcus, N. L. Chemistry of Nitrogen Radicals. VI. The Free-Radical Addition of Dialkyl-N-Chloramines to Substituted Olefins. *J. Org. Chem.* **1967**, *32* (11), 3273–3284. https://doi.org/10.1021/jo01286a002.

(20) Stein, C.; Tyler, J. L.; Wiener, J.; Boser, F.; Daniliuc, C. G.; Glorius, F. Anomeric Amide-Enabled Alkene-Arene and Alkene-Alkene Aminative Coupling. *Angew Chem Int Ed* **2025**, *64* (5), e202418141. https://doi.org/10.1002/anie.202418141.

(21) Constantinou, C. T.; Gkizis, P. L.; Lagopanagiotopoulou, O. T. G.; Skolia, E.; Nikitas, N. F.; Triandafillidi, I.; Kokotos, C. G. Photochemical Aminochlorination of Alkenes without the Use of an External Catalyst. *Chemistry A European J* **2023**, *29* (45), e202301268. https://doi.org/10.1002/chem.202301268.

(22) Šakić, D.; Zipse, H. Radical Stability as a Guideline in C-H Amination Reactions. *Adv. Synth. Catal.* **2016**, *358* (24), 3983–3991. https://doi.org/10.1002/adsc.201600629.

(23) Hioe, J.; Šakić, D.; Vrček, V.; Zipse, H. The Stability of Nitrogen-Centered Radicals. *Org. Biomol. Chem.* **2015**, *13* (1), 157–169. https://doi.org/10.1039/C4OB01656D.

(24) Hioe, J.; Zipse, H. Radical Stability—Thermochemical Aspects. In *Encyclopedia of Radicals in Chemistry, Biology and Materials*; Chatgilialoglu, C., Studer, A., Eds.; Wiley, 2012. https://doi.org/10.1002/9781119953678.rad012.

(25) Shkunnikova, S.; Zipse, H.; Šakić, D. Role of Substituents in the Hofmann–Löffler–Freytag Reaction. A Quantum-Chemical Case Study on Nicotine Synthesis. *Org. Biomol. Chem.* **2021**, *19* (4), 854–865. https://doi.org/10.1039/D0OB02187C.

(26) Zhang, H.; Muñiz, K. Selective Piperidine Synthesis Exploiting Iodine-Catalyzed C_{sp^3}–H Amination under Visible Light. *ACS Catal.* **2017**, *7* (6), 4122–4125. https://doi.org/10.1021/acscatal.7b00928.

(27) Short, M. A.; Shehata, M. F.; Sanders, M. A.; Roizen, J. L. Sulfamides Direct Radical-Mediated Chlorination of Aliphatic C–H Bonds. *Chem. Sci.* **2020**, *11* (1), 217–223. https://doi.org/10.1039/C9SC03428E.

(28) Short, M. A.; Blackburn, J. M.; Roizen, J. L. Sulfamate Esters Guide Selective Radical-Mediated Chlorination of Aliphatic C−H Bonds. *Angew. Chem. Int. Ed.* **2018**, *57* (1), 296–299. https://doi.org/10.1002/anie.201710322.
(29) Short, M. A.; Blackburn, J. M.; Roizen, J. L. Modifying Positional Selectivity in C–H Functionalization Reactions with Nitrogen-Centered Radicals: Generalizable Approaches to 1,6-Hydrogen-Atom Transfer Processes. *Synlett* **2020**, *31* (02), 102–116. https://doi.org/10.1055/s-0039-1691501.
(30) Short, M. A.; Shehata, M. F.; Sanders, M. A.; Roizen, J. L. Sulfamides Direct Radical-Mediated Chlorination of Aliphatic C–H Bonds. *Chem. Sci.* **2020**, *11* (1), 217–223. https://doi.org/10.1039/C9SC03428E.
(31) Sutcliffe, R.; Ingold, K. U. Kinetic Applications of Electron Paramagnetic Resonance Spectroscopy. 40. Intramolecular Reactions of Some N-Alkylcarboxamidyl Radicals. *J. Am. Chem. Soc.* **1982**, *104* (22), 6071–6075. https://doi.org/10.1021/ja00386a038.
(32) Rice, F. O.; Grelecki, C. J. The Dimethylamino Radical. *J. Am. Chem. Soc.* **1957**, *79* (11), 2679–2680. https://doi.org/10.1021/ja01568a004.
(33) Y.-R. Luo, Comprehensive Handbook of Chemical Bond Energies, CRC Press, London, **2007**.
(34) Musa, O. M.; Horner, J. H.; Shahin, H.; Newcomb, M. A Kinetic Scale for Dialkylaminyl Radical Reactions. *J. Am. Chem. Soc.* **1996**, *118* (16), 3862–3868. https://doi.org/10.1021/ja954268f.
(35) Esker, J. L.; Newcomb, M. Chemistry of Amidyl Radicals Produced from N-Hydroxypyridine-2-Thione Imidate Esters. *J. Org. Chem.* **1993**, *58* (18), 4933–4940. https://doi.org/10.1021/jo00070a033.
(36) Horner, J. H.; Musa, O. M.; Bouvier, A.; Newcomb, M. Absolute Kinetics of Amidyl Radical Reactions. *J. Am. Chem. Soc.* **1998**, *120* (31), 7738–7748. https://doi.org/10.1021/ja981244a.
(37) Le Tadic-Biadatti, M.-H.; Callier-Dublanchet, A.-C.; Horner, J. H.; Quiclet-Sire, B.; Zard, S. Z.; Newcomb, M. Absolute Rate Constants for Iminyl Radical Reactions. *J. Org. Chem.* **1997**, *62* (3), 559–563. https://doi.org/10.1021/jo961530+.
(38) Nagano, M.; Suzuki, T.; Ichimura, T.; Okutsu, T.; Hiratsuka, H.; Kawauchi, S. Production and Excited State Dynamics of the Photorearranged Isomer of Benzyl Chloride and Its Methyl Derivatives Studied by Stepwise Two-Color Laser Excitation Transient Absorption and Time-Resolved Thermal Lensing Techniques. *J. Phys. Chem. A* **2005**, *109* (26), 5825–5831. https://doi.org/10.1021/jp051183k.
(39) Kozuch, S. Steady State Kinetics of Any Catalytic Network: Graph Theory, the Energy Span Model, the Analogy between Catalysis and Electrical Circuits, and the Meaning of "Mechanism." *ACS Catal.* **2015**, *5* (9), 5242–5255. https://doi.org/10.1021/acscatal.5b00694.
(40) Perez-Benito, J. F. Some Considerations on the Fundamentals of Chemical Kinetics: Steady State, Quasi-Equilibrium, and Transition State Theory. *J. Chem. Educ.* **2017**, *94* (9), 1238–1246. https://doi.org/10.1021/acs.jchemed.6b00957.
(41) Willcott, M. R. MestRe Nova. *J. Am. Chem. Soc.* **2009**, *131* (36), 13180–13180. https://doi.org/10.1021/ja906709t.
(42) Stoll, S.; Schweiger, A. EasySpin, a Comprehensive Software Package for Spectral Simulation and Analysis in EPR. *Journal of Magnetic Resonance* **2006**, *178* (1), 42–55. https://doi.org/10.1016/j.jmr.2005.08.013.

(43) Šakić, D. DSakicLab/visualEPR, 2023. https://github.com/DSakicLab/visualEPR (accessed 2024-10-30).
(44) Pracht, P.; Bohle, F.; Grimme, S. Automated Exploration of the Low-Energy Chemical Space with Fast Quantum Chemical Methods. *Phys. Chem. Chem. Phys.* **2020**, *22* (14), 7169–7192. https://doi.org/10.1039/C9CP06869D.
(45) Bannwarth, C.; Caldeweyher, E.; Ehlert, S.; Hansen, A.; Pracht, P.; Seibert, J.; Spicher, S.; Grimme, S. Extended TIGHT-BINDING Quantum Chemistry Methods. *WIREs Comput Mol Sci* **2021**, *11* (2), e1493. https://doi.org/10.1002/wcms.1493.
(46) Bannwarth, C.; Ehlert, S.; Grimme, S. GFN2-xTB—An Accurate and Broadly Parametrized Self-Consistent Tight-Binding Quantum Chemical Method with Multipole Electrostatics and Density-Dependent Dispersion Contributions. *J. Chem. Theory Comput.* **2019**, *15* (3), 1652–1671. https://doi.org/10.1021/acs.jctc.8b01176.
(47) Becke, A. D. Density-Functional Thermochemistry. III. The Role of Exact Exchange. *The Journal of Chemical Physics* **1993**, *98* (7), 5648–5652. https://doi.org/10.1063/1.464913.
(48) Stephens, P. J.; Devlin, F. J.; Chabalowski, C. F.; Frisch, M. J. Ab Initio Calculation of Vibrational Absorption and Circular Dichroism Spectra Using Density Functional Force Fields. *J. Phys. Chem.* **1994**, *98* (45), 11623–11627. https://doi.org/10.1021/j100096a001.
(49) Ditchfield, R.; Hehre, W. J.; Pople, J. A. Self-Consistent Molecular-Orbital Methods. IX. An Extended Gaussian-Type Basis for Molecular-Orbital Studies of Organic Molecules. *The Journal of Chemical Physics* **1971**, *54* (2), 724–728. https://doi.org/10.1063/1.1674902.
(50) Marenich, A. V.; Cramer, C. J.; Truhlar, D. G. Universal Solvation Model Based on Solute Electron Density and on a Continuum Model of the Solvent Defined by the Bulk Dielectric Constant and Atomic Surface Tensions. *J. Phys. Chem. B* **2009**, *113* (18), 6378–6396. https://doi.org/10.1021/jp810292n.
(51) Mennucci, B.; Tomasi, J.; Cammi, R.; Cheeseman, J. R.; Frisch, M. J.; Devlin, F. J.; Gabriel, S.; Stephens, P. J. Polarizable Continuum Model (PCM) Calculations of Solvent Effects on Optical Rotations of Chiral Molecules. *J. Phys. Chem. A* **2002**, *106* (25), 6102–6113. https://doi.org/10.1021/jp020124t.
(52) Grimme, S. Semiempirical Hybrid Density Functional with Perturbative Second-Order Correlation. *The Journal of Chemical Physics* **2006**, *124* (3), 034108. https://doi.org/10.1063/1.2148954.
(53) Neese, F.; Schwabe, T.; Grimme, S. Analytic Derivatives for Perturbatively Corrected "Double Hybrid" Density Functionals: Theory, Implementation, and Applications. *The Journal of Chemical Physics* **2007**, *126* (12), 124115. https://doi.org/10.1063/1.2712433.
(54) Curtiss, L. A.; Redfern, P. C.; Raghavachari, K.; Rassolov, V.; Pople, J. A. Gaussian-3 Theory Using Reduced Mo/Ller-Plesset Order. *The Journal of Chemical Physics* **1999**, *110* (10), 4703–4709. https://doi.org/10.1063/1.478385.
(55) Grimme, S.; Antony, J.; Ehrlich, S.; Krieg, H. A Consistent and Accurate *Ab Initio* Parametrization of Density Functional Dispersion Correction (DFT-D) for the 94 Elements H-Pu. *The Journal of Chemical Physics* **2010**, *132* (15), 154104. https://doi.org/10.1063/1.3382344.
(56) Hill, T.L. *An Introduction to Statistical Thermodynamics.* 1st Edition; Dover Publications Inc., New York, 1986.
(57) Steinfeld, J.I., Francisco, J.S., Hase, W.L. *Chemical Kinetics and Dynamics.* 2nd Illustrated Edition; Prentice Hall, 1999.

(58) Vrček, I. V.; Šakić, D.; Vrček, V.; Zipse, H.; Biruš, M. Computational Study of Radicals Derived from Hydroxyurea and Its Methylated Analogues. *Org. Biomol. Chem.* **2012**, *10* (6), 1196–1206. https://doi.org/10.1039/C1OB06594G.
(59) Hermosilla, L.; Calle, P.; García De La Vega, J. M.; Sieiro, C. Density Functional Theory Study of ^{14} N Isotropic Hyperfine Coupling Constants of Organic Radicals. *J. Phys. Chem. A* **2006**, *110* (50), 13600–13608. https://doi.org/10.1021/jp064900z.
(60) Frisch, M. J.; Trucks, G. W.; Schlegel, H. B.; Scuseria, G. E.; Robb, M. A.; Cheeseman, J. R.; Scalmani, G.; Barone, V.; Petersson, G. A.; Nakatsuji, H.; et al. Gaussian 16, Revision C. 01. Gaussian, Inc.: Wallingford CT, 2016.
(61) HR-ZOO, Cluster Supek; University of Zagreb University Computing Centre SRCE. KK.01.1.1.08.0001, EU Funded within OPCC for Republic of Croatia: Zagreb, 2023.
(62) PharmInova Project, Cluster Sw.Pharma.Hr. University of Zagreb Faculty of Pharmacy and Biochemistry. KK.01.1.1.02.0021, EU Funded by the European Regional Development Fund: Zagreb 2023.).
(63) Bauernschmitt, R.; Häser, M.; Treutler, O.; Ahlrichs, R. Calculation of Excitation Energies within Time-Dependent Density Functional Theory Using Auxiliary Basis Set Expansions. *Chemical Physics Letters* **1997**, *264* (6), 573–578. https://doi.org/10.1016/S0009-2614(96)01343-7.
(64) Yanai, T.; Tew, D. P.; Handy, N. C. A New Hybrid Exchange–Correlation Functional Using the Coulomb-Attenuating Method (CAM-B3LYP). *Chemical Physics Letters* **2004**, *393* (1–3), 51–57. https://doi.org/10.1016/j.cplett.2004.06.011.
(65) Ardura, D.; López, R.; Sordo, T. L. Relative Gibbs Energies in Solution through Continuum Models: Effect of the Loss of Translational Degrees of Freedom in Bimolecular Reactions on Gibbs Energy Barriers. *J. Phys. Chem. B* **2005**, *109* (49), 23618–23623. https://doi.org/10.1021/jp0540499.
(66) Šakić, D.; Šonjić, P.; Tandarić, T.; Vrček, V. Chlorination of *N* -Methylacetamide and Amide-Containing Pharmaceuticals. Quantum-Chemical Study of the Reaction Mechanism. *J. Phys. Chem. A* **2014**, *118* (12), 2367–2376. https://doi.org/10.1021/jp5012846.
(67) El-Ajou, A.; Al-ghananeem, H.; Saadeh, R.; Qazza, A.; Oqielat Moa'ath N. A modern analytic method to solve singular and non-singular linear and non-linear differential equations. *Front. Phys.* **2023**, *11*, 1–13. https://doi.org/ 10.3389/fphy.2023.1167797
(68) Cheng, C. M.; Peng, Z. K.; Zhang, W. M.; Meng, G. Volterra-Series-Based Nonlinear System Modeling and Its Engineering Applications: A State-of-the-Art Review. *Mechanical Systems and Signal Processing* **2017**, *87*, 340–364. https://doi.org/10.1016/j.ymssp.2016.10.029.
(69) Gavalas, G. R. *Nonlinear Differential Equations of Chemically Reacting Systems*; Coleman, B. D., Aris, R., Collatz, L., Ericksen, J. L., Germain, P., Gurtin, M. E., Schiffer, M. M., Sternberg, E., Truesdell, C., Series Eds.; Springer Tracts in Natural Philosophy; Springer Berlin Heidelberg: Berlin, Heidelberg, **1968**; Vol. 17. https://doi.org/10.1007/978-3-642-87643-1.
(70) Pachpatte, B. G. *Mathematics in Science and Engineering: Nonlinear Integral Inequalities I.* 197; Elsevier, **1998**. https://doi.org/10.1016/S0076-5392(98)80004-0
(71) Wang, W.-S.; Li, S.-F.; Su, K. Nonlinear Stability of Runge–Kutta Methods for Neutral Delay Differential Equations. *Journal of Computational and Applied Mathematics* **2008**, *214* (1), 175–185. https://doi.org/10.1016/j.cam.2007.02.031.

(72) Zennaro, M. Asymptotic Stability Analysis of Runge-Kutta Methods for Nonlinear Systems of Delay Differential Equations. *Numerische Mathematik* **1997**, *77* (4), 549–563. https://doi.org/10.1007/s002110050300.
(73) Iserles, A. Stability and Dynamics of Numerical Methods for Nonlinear Ordinary Differential Equations. *IMA J Numer Anal* **1990**, *10* (1), 1–30. https://doi.org/10.1093/imanum/10.1.1.
(74) Ricardo, H. J. Systems of Nonlinear Differential Equations. In *A Modern Introduction to Differential Equations*; Elsevier, 2021; pp 361–420. https://doi.org/10.1016/B978-0-12-818217-8.00014-2.